Energy barrier for ion field emission from a dielectric liquid sphere

Marco Magnani and Manuel Gamero-Castaño
Department of Mechanical and Aerospace Engineering, University of California, Irvine, California 92697, USA

(Received 14 October 2021; revised 23 April 2022; accepted 25 April 2022; published 11 May 2022)

Ion field emission from the surface of a dielectric liquid is commonly modeled as a kinetic process with an energy barrier lowered by the strength of the electric field. Expressions for the energy barrier exist for simplified cases such as a planar surface and a conducting sphere. This article derives an analytical expression for the more general case of a dielectric sphere, which is the continuum model and geometry for most cases of interest. The energy barrier is computed using the method of image charges, and compared to existing expressions for simpler models. The energy barrier increases at decreasing dielectric constant and decreasing radius of curvature. Ion emission from typical systems (the ideal Taylor cone and charged nanodroplets) differs substantially when calculated with either our model or with existing simpler models.

DOI: 10.1103/PhysRevE.105.054802

I. INTRODUCTION

Ion evaporation is the spontaneous emission of ions from a surface. The emission rate depends on the properties of the surface, the emitted ion, and the temperature. It is enhanced by the presence of an electric field, in which case the process is referred to as ion field emission. Müller [1,2] first studied ion field emission from metallic surfaces, explaining it as the interaction between the ion and the electric field including that of the image charge induced by the emitted ion. Gomer [3] proposed an alternative model that regards the emission as the transition between two competing energy states. This approach is more challenging because it requires a quantum-mechanical treatment of the process.

Ion field emission from dielectric liquids occurs naturally in aerosols. It is a key element in electrospray mass spectrometry [4], where the combination of ion emission and Coulomb explosions from charged droplets in the aerosol determines the net charge of the particle analyzed by the mass spectrometer, typically a macromolecule or a cluster [5]. Ion field emission is routinely observed and investigated by electrospraying dielectric liquids with high electrical conductivity, using both experimental and numerical approaches [6,7]. Two distinct cases occur: electrosprays operating in the cone-jet mode produce a thin jet that breaks into droplets, and ion emission can take place from both the jet and droplets leading to a mixed droplet-ion emission regime [8]; ion emission can also take place from the tip of the liquid meniscus, or Taylor cone, in the absence of jet and droplet formation, leading to a purely ionic emission regime [9,10]. In either case the electrospray provides a stationary geometry for the emission of ions, and by measuring the emitted current and calculating the electric field, field emission models can be studied [11,12]. This soft ionization technique does not require the use of a plasma discharge chamber; it operates at a low power level per emitter, it efficiently converts electric power into beam kinetic power, and micromachining techniques can be used to create dense emitter arrays. These properties make this ion source ideal for space propulsion, especially for SmallSats (spacecrafts weighing less than 600 kg). The number of launched SmallSats has grown significantly in the past few years, from 126 in 2016 to 389 in 2019 and 1743 in 2021 [13], and since most of them are intended for telecommunication applications, onboard propulsion for orbit insertion and maintenance is an enabling capability [14]. Chemical propulsion is not ideal because of its relatively low specific impulse, while conventional electric propulsion cannot be scaled down to operate at the power levels of SmallSats [15,16]. Electrospray propulsion is expected to fill the propulsion need of SmallSats [17–19], and a precise fundamental understanding of ion field emission, which is one of its key ionization mechanism, is needed to advance this technology.

Iribarne and Thomson [20] developed the following equation for ion field emission from a liquid:

$$J = \frac{k_B T}{h}\sigma \exp\left(-\frac{\Delta G_0^S - G(E)}{k_B T}\right), \tag{1}$$

where J is the ion current density, h and k_B are the Planck and Boltzmann constants, T is the temperature at the emitting surface, and σ is the surface charge density. ΔG_0^S is the free enthalpy of solution of the ion, and $G(E)$ is the electrostatic contribution to the enthalpy. The difference between these two terms is the energy barrier that the ion must overcome to escape the surface. ΔG_0^S is a property of the liquid and ion pair, while $G(E)$ is a function of the electric field. As the ion moves away from the surface, it is repelled by the electric field induced by the net charge distributed over the surface (it has the same polarity as the ion), and attracted by the field of the image charge it induces. The combined effect reduces the intrinsic energy barrier ΔG_0^S by the amount $G(E)$. Iribarne and Thomson used the image charge method to compute $G(E)$ for the case of a perfect conductor with a planar surface, a calculation that is easily extended to dielectrics.

 ©2022 American Physical Society

Gamero-Castaño and de la Mora [5] used the same model to compute $G(E)$ for a conducting sphere.

The ion evaporation rate depends exponentially on $G(E)$, and therefore using a physical model that closely resembles the emitting surface is key for accurate predictions. In the case of dielectric liquids, the high electric fields required for emission can only be produced from surfaces with radii of curvature of at most a few tens of nanometers. Naturally emitting geometries include the highly charged nanodroplets and nanojets of electrosprays [21]. In these cases, retaining both the curvature of the surface and the dielectric nature of the liquid are key for computing $G(E)$. This article derives this more general form of the energy barrier, and compares it to existing formulations based on excessively simplifying assumptions (e.g., a planar and/or equipotential surface).

II. EMISSION FROM A SURFACE WITH FINITE RADIUS OF CURVATURE AND DIELECTRIC CONSTANT

To model the local behavior of a curved surface, we consider an ion-emitting dielectric sphere of radius R, centered in a spherical coordinate system $\{r, \theta, \phi\}$. The electric potential induced by the charged sphere is given by

$$\Phi_{\text{surf}}(r) = \frac{R^2 E_s}{r}, \tag{2}$$

where E_s is the electric field on the surface associated with the net charge. The emitted ion is modeled as a point charge q located at $\{r_i, 0, 0\}$. Under these conditions, the electric potential of the image charge induced by the ion and distributed inside the sphere is [22]

$$\Phi_{\text{imag}}(r,\theta) = \begin{cases} -\frac{q}{4\pi\varepsilon_0 r_i}\sum_{n=1}^{\infty}\frac{n(\varepsilon-1)}{n(\varepsilon+1)+1}\left(\frac{r}{r_i}\right)^n P_n(\cos\theta), & r < R, \\ -\frac{q}{4\pi\varepsilon_0 R}\sum_{n=1}^{\infty}\frac{n(\varepsilon-1)}{n(\varepsilon+1)+1}\left(\frac{R^2}{r_i r}\right)^{n+1} P_n(\cos\theta), & r \geqslant R, \end{cases} \tag{3}$$

where P_n are the Legendre polynomials of integer order n. The net value of the image charge is zero, as can be shown by applying Gauss's law to the electric field associated with (3). Since all the calculations are done along the line of sight of the emitted ion, (3) is simplified by considering $\theta = 0$. The radial component of the electric field along the path of the ion is then

$$E_{\text{imag}}(r) = \begin{cases} \frac{q}{4\pi\varepsilon_0 r_i}\sum_{n=1}^{\infty}\frac{n^2(\varepsilon-1)}{n(\varepsilon+1)+1}\frac{r^{n-1}}{r_i{}^n}, & r < R, \\ -\frac{q}{4\pi\varepsilon_0 R}\sum_{n=1}^{\infty}\frac{n(n+1)(\varepsilon-1)}{n(\varepsilon+1)+1}\frac{1}{r^{n+2}}\left(\frac{R^2}{r_i}\right)^{n+1}, & r \geqslant R. \end{cases} \tag{4}$$

The total force acting on the ion is the repulsive, spherically symmetric force induced by the net charge on the surface of the sphere, plus the attractive force induced by the image charge:

$$F_{\text{ion}}(r_i) = q[E_{\text{surf}}(r_i) + E_{\text{imag}}(r_i)], \tag{5}$$

$$F_{\text{ion}}(r_i) = \frac{qR^2E_s}{r_i{}^2} - \frac{q^2}{4\pi\varepsilon_0 R}\sum_{n=1}^{\infty}\frac{n(n+1)(\varepsilon-1)}{n(\varepsilon+1)+1}\frac{R^{2n+2}}{r_i{}^{2n+3}}. \tag{6}$$

The force of the net charge repels the ion away from the surface, while the force of the image charge attracts it and is the dominant term near the surface. The potential energy of the ion as it moves away from the sphere is

$$U_{\text{ion}}(r) = -\int_{\infty}^{r} F_{\text{ion}}(\xi)d\xi = \frac{qR^2E_s}{r} - \frac{q^2}{8\pi\varepsilon_0 R}\sum_{n=1}^{\infty}\frac{n(\varepsilon-1)}{n(\varepsilon+1)+1}\left(\frac{R}{r}\right)^{2n+2}. \tag{7}$$

The steps taken from Eq. (3) to (7) are necessary to obtain the correct potential energy of the ion. It would appear that the successive differentiation and integration yielding (4) and (7), respectively, are redundant and that the energy of the ion could be directly obtained by adding (2) and (3). However, note that (3) is larger than the term in (7) associated with the image charge by a factor of 2. This is due to the use of the radial coordinate r to perform the first differentiation yielding the electric field (4), while the final integration leading to (7) is instead done on the ion position r_i, now with $r = r_i$.

Figure 1 shows the potential energy of the ion, together with its components associated with the image charge and the net charge on the surface, as a function of the distance x from the surface ($r = R + x$). The potential exhibits a maximum at r^*. The energy barrier is the difference between this maximum and the energy at the surface, $U_{\text{ion}}(r^*) - U_{\text{ion}}(R)$. Note that the potential induced by the image charge goes to minus infinity as the ion approaches the surface, seemingly making the energy barrier infinite. In reality, the use of the image charge potential to model the interaction between the ion and the uncharged dielectric breaks down within atomic distances

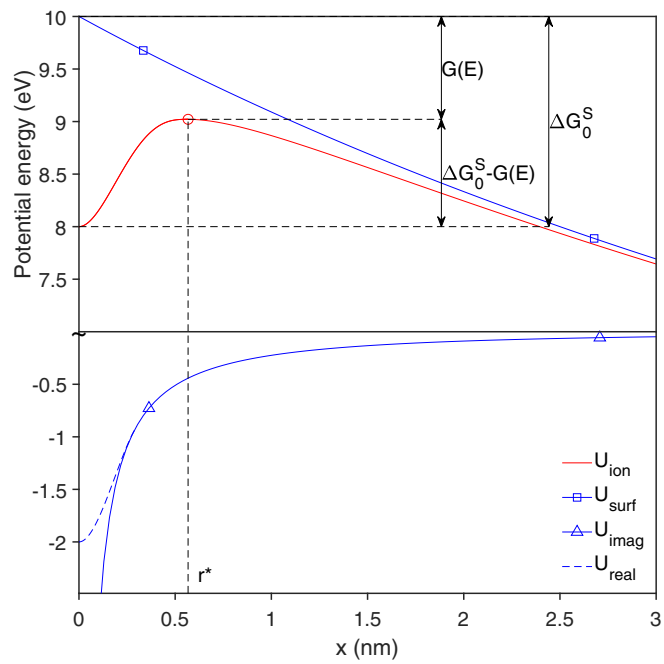

FIG. 1. Potential energy of an ion as a function of its distance from the surface of a dielectric and charged sphere, for $R = 10$ nm, $\varepsilon = 10$, $E_s = 1$ V/nm, and $\Delta G_0^S = 2$ eV. The red curve (U_{ion}) is the net potential energy, i.e., the sum of the potential energies induced by the net charge (U_{surf}) and the image charge (U_{imag}). Near the surface, the image charge model breaks down, and the interaction energy tends to $-\Delta G_0^S$ (U_{real}).

from the surface, and more complicated models/potentials are needed to obtain the correct value of the ion energy at the surface, namely $-\Delta G_0^S$. This is illustrated in Fig. 1 with the insertion of an ad hoc dashed segment that takes the interaction between the ion and the uncharged dielectric to the correct value at the surface. Figure 1 shows that, in the absence of net charge, the energy barrier is simply ΔG_0^S, and when net charge is present on the surface, its associated electric field reduces this energy barrier in the amount $G(E)$:

$$\begin{aligned} G(E) &= \Delta G_0^S - [U_{\rm ion}(r^*) - U_{\rm ion}(R)] \\ &= q\int_R^{r^*} E_{\rm surf}(\xi)d\xi + q\int_\infty^{r^*} E_{\rm imag}(\xi)d\xi \\ &= \left(1-\frac{R}{r^*}\right)qRE_s + \frac{q^2(\varepsilon-1)}{8\pi\varepsilon_0 R}\sum_{n=1}^{\infty}\frac{1}{\varepsilon+1+\frac{1}{n}}\left(\frac{R}{r^*}\right)^{2n+2}. \end{aligned} \tag{8}$$

This calculation of $G(E)$ assumes that the potential of the image charge accurately describes the interaction between the ion and the uncharged dielectric near r^*, i.e., near the position of the maximum of the potential. We also note that the series in (8) has a poor convergence for a large radius of curvature, and its numerical calculation requires a large number of terms. We can estimate the number of terms needed for a certain accuracy by checking the relative magnitude of the first and the "last" term of the series:

$$\mathcal{E} \cong \frac{\frac{1}{\varepsilon+1+\frac{1}{n_\infty}}\left(\frac{R}{r^*}\right)^{2n_\infty+2}}{\frac{1}{\varepsilon+2}\left(\frac{R}{r^*}\right)^4}. \tag{9}$$

Assuming that n_∞ is a large number and that the dielectric constant is fairly bigger than 1, we obtain that to get an error on the infinite sum of the order of $\mathcal{E}$ we need to consider approximately

$$n_\infty \cong \frac{\ln \mathcal{E}}{2\ln\frac{R}{r^*}} \tag{10}$$

terms in the sum. It is clear that when $R \to \infty$, the denominator of (10) goes to zero since $r^* = R + x^*$, blowing up the number of terms needed to evaluate the series. Under these conditions, it may be computationally better to switch to the classic dielectric plane approximation for $G(E)$.

III. COMPARISON WITH EXISTING MODELS

We next compare (8) with the values for limiting cases frequently used in the literature. The potential energies of an ion emitted from a planar conductor, a planar dielectric, and a spherical conductor are given, respectively, by

$$U_{\rm ion}^{\rm pc}(x) = qE_s x + \frac{q^2}{16\pi\varepsilon_0 x}, \tag{11}$$

$$U_{\rm ion}^{\rm pd}(x) = qE_s x + \frac{(\varepsilon-1)q^2}{16\pi\varepsilon_0(\varepsilon+1)x}, \tag{12}$$

$$U_{\rm ion}^{\rm sc}(r) = \left(1-\frac{R}{r}\right)qRE_s + \left(\frac{1}{R}-\frac{R}{r^2}+\frac{R}{r^2-R^2}\right)\frac{q^2}{8\pi\varepsilon_0}. \tag{13}$$

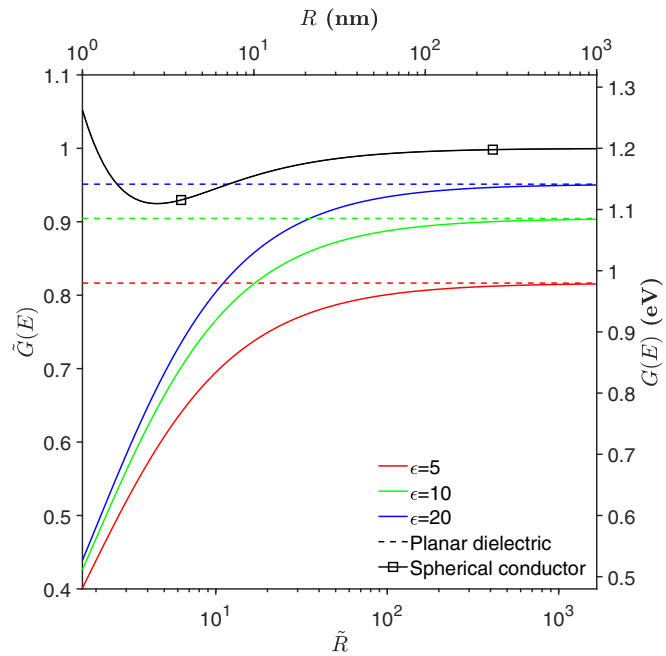

FIG. 2. Dimensionless reduction of the energy barrier, Eq. (16), for several values of the dielectric constant. The reduction for a planar dielectric and a spherical conductor are also plotted for comparison. We provide coordinates in physical units for an electric field $E_s = 1$ V/nm (for this condition, the characteristic energy and length are $U_c = 1.2$ eV and $L_c = 0.6$ nm).

x stands for the distance between the ion and the emitting surface. The electrostatic reductions of the energy barrier in the first two cases are

$$G^{\rm pc}(E) = \sqrt{\frac{q^3E_s}{4\pi\varepsilon_0}}, \tag{14}$$

$$G^{\rm pd}(E) = \sqrt{\frac{q^3E_s(\varepsilon-1)}{4\pi\varepsilon_0(\varepsilon+1)}}, \tag{15}$$

while the electrostatic reduction for the spherical conductor, $G^{\rm sc}(E)$, needs to be obtained numerically. The comparison is more easily done by making these functions dimensionless using the electrostatic reduction for a planar conductor and its position as the characteristic energy and length, respectively, $U_c = (q^3E_s/4\pi\varepsilon_0)^{1/2}$ and $L_c = (q/16\pi\varepsilon_0E_s)^{1/2}$. In particular, the dimensionless form of (8) is

$$\tilde{G}(E) = \left(1-\frac{\tilde{R}}{\tilde{r}^*}\right)\frac{\tilde{R}}{2} + \frac{1}{\tilde{R}}\sum_{n=1}^{\infty}\frac{\varepsilon-1}{\varepsilon+1+\frac{1}{n}}\left(\frac{\tilde{R}}{\tilde{r}^*}\right)^{2n+2}. \tag{16}$$

Figure 2 plots $\tilde{G}(E)$ as a function of the dimensionless radius of curvature and for several values of the dielectric constant. It also shows the dimensionless values for a planar dielectric with the same values of the dielectric constant, as well as for a spherical conductor as a function of $\tilde{R}$. In all cases, the values are smaller than 1, i.e., a flat conductor yields the largest electrostatic reduction of the energy barrier. The electrostatic reduction of the energy barrier decreases significantly as the radius of curvature becomes smaller, and the smaller the dielectric constant, the smaller is the reduction of the energy

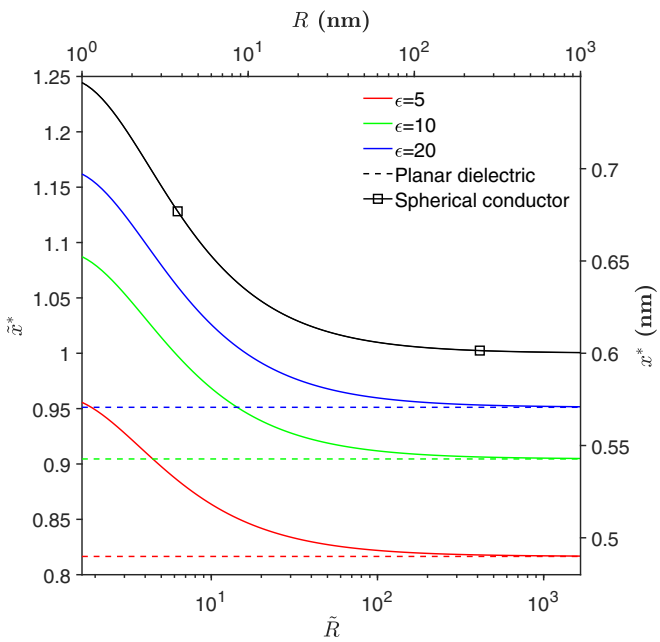

FIG. 3. Dimensionless distance between the energy maximum and the surface as a function of the dimensionless radius of curvature and dielectric constant. We also plot the distance in physical units for an electric field on the surface $E_s = 1$ V/nm (for this condition, the characteristic energy and length are $U_c = 1.2$ eV and $L_c = 0.6$ nm).

barrier. The simplest planar conductor model is commonly used to estimate ion field emission regardless of the dielectric nature and curvature of the emitting substrate, but this choice clearly overestimates the intensity of ion emission. Note also that, for a given dielectric constant, the values of $\tilde{G}(E)$ at large radius of curvature asymptote to the values for the planar dielectric, and that the curve for the spherical conductor is an upper limit for $\tilde{G}(E)$ at large dielectric constant. This is to be expected because (8) is a general solution, and expressions for limiting cases such as a perfect conductor and a planar dielectric surface can be derived from it.

Figure 3 shows the dimensionless distance between the emitting surface and the position of the energy maximum, $\tilde{x}^*$. The distance increases with the dielectric constant and as the radius of curvature becomes smaller. As mentioned earlier, the calculation of $G(E)$ assumes that the image charge potential is a valid description of the interaction between the ion and the uncharged dielectric near the maximum of the potential energy. Thus, Fig. 3 suggests that the smaller the radius of curvature and the larger the dielectric constant, the more valid the classical formulation of ion emission. We expect the classical formulation to be valid in most cases of ion emission from liquids of interest. For example, EMI-Im, a typical ionic liquid used in electrospray research [21], has a dielectric constant of 12, and for a typical ion-emitting droplet with a radius of 10 nm, the separation between the potential maximum and the surface is 0.58 nm. The estimated radius of the EMI-Im molecule is 0.3 nm [23,24]. Thus, although within a distance of 0.3 nm from the surface the image charge potential is probably a poor approximation of the interaction, the separation of 0.58 nm between the energy barrier and the surface suggests that the image charge potential is a valid approximation to compute $G(E)$. Finally, note that the values of $\tilde{x}^*$ are generally close to 1. In this case, (16) can be simplified by taking $\tilde{r}^* = \tilde{R} + 1$, yielding an expression with an explicit dependence on $\tilde{R}$ and ε,

$$\tilde{G}(E) \cong \frac{1}{2(1+1/\tilde{R})} + \frac{1}{\tilde{R}} \sum_{n=1}^{\infty} \frac{\varepsilon - 1}{\varepsilon + 1 + \frac{1}{n}} \left(\frac{1}{1+1/\tilde{R}} \right)^{2n+2}, \tag{17}$$

and for which, unlike in (16), there is no need to first compute numerically $\tilde{r}^*(\tilde{R}, \varepsilon)$ to evaluate $\tilde{G}(E)$.

IV. EFFECT OF THE ENERGY REDUCTION MODEL IN THE EMISSION FROM TYPICAL GEOMETRIES

In this section, we analyze the differences in ion emission associated with our model and the previous planar/conductor models. We consider two analytic scenarios: ion emission from the tip of an ideal Taylor cone, and ion emission from a spherical droplet charged at the Rayleigh limit. In both cases, the radius of curvature of the emitting surface can be a few nanometers, i.e., in the range where Eq. (8) departs significantly from the frequently used planar approximations.

A Taylor cone is an analytic solution for a static and electrified liquid meniscus where the electric and capillary stresses are perfectly balanced [25]. The meniscus adopts a semi-infinite conical shape with a half-angle $\theta^T = 49.29°$. The liquid meniscus is equipotential, and the electric field on the surface is

$$E_s^T(\rho) = \sqrt{\frac{2\gamma}{\varepsilon_0} \frac{\cos\theta^T}{\rho}}, \tag{18}$$

where γ is the surface tension of the liquid, and ρ is the radial coordinate in a cylindrical frame of reference centered at the vertex. The surface charge is equal to $\varepsilon_0 E_s^T$, and the average radius of curvature of the cone is

$$R^T(\rho) = \frac{2\rho}{\cos\theta^T}. \tag{19}$$

These values for the electric field, radius of curvature, and surface charge, inserted in Eq. (1), and the expressions for $G(E)$ yield the ion current emitted from an ideal Taylor cone. Figure 4 shows the current density as a function of the radial distance (cylindrical coordinates) from the tip, computed with our spherical dielectric model for the reduction of the energy barrier and several values of the dielectric constant. For comparison, the ion current density is also calculated using the planar dielectric and the spherical conductor models. Table I provides the total ion current emitted in each case. The electric field on the surface of an ideal Taylor cone scales as $\rho^{-1/2}$, tending to infinity towards the vertex. On the other hand, the mean radius of curvature scales as ρ. When both limiting behaviors are inserted in our spherical dielectric model, e.g., using Eq. (17) for an explicit approximation, the reduction of the dimensionless energy barrier scales as $\tilde{G}(E) \propto \tilde{R}$, while its dimensional form scales as $G(E) \propto \rho^{1/2}$. Thus, as the vertex is approached, the reduction of the energy barrier tends to zero even though the electric field tends to infinity, effectively suppressing ion field emission. On the other hand, Fig. 2

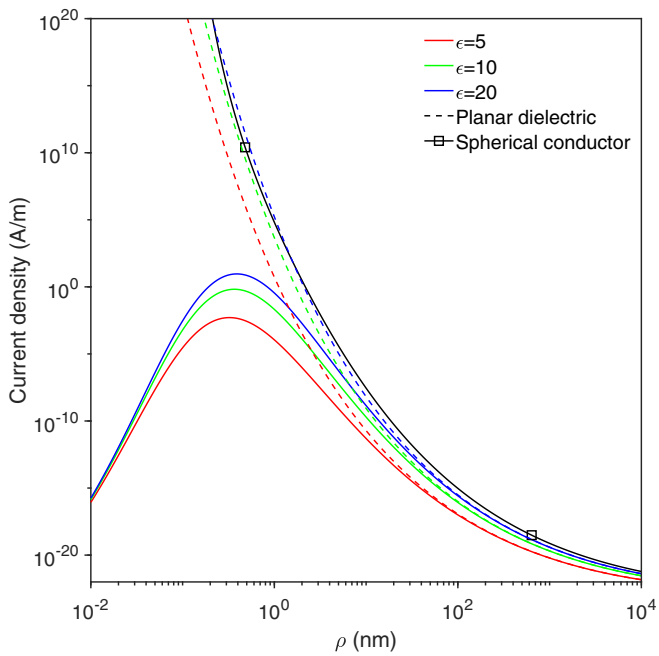

FIG. 4. Ion current density along the surface of an ideal Taylor cone. We use a temperature of 25 °C, a surface tension of 0.05 J/m^2, and a free enthalpy of solution $\Delta G_0^S = 1.7$ eV.

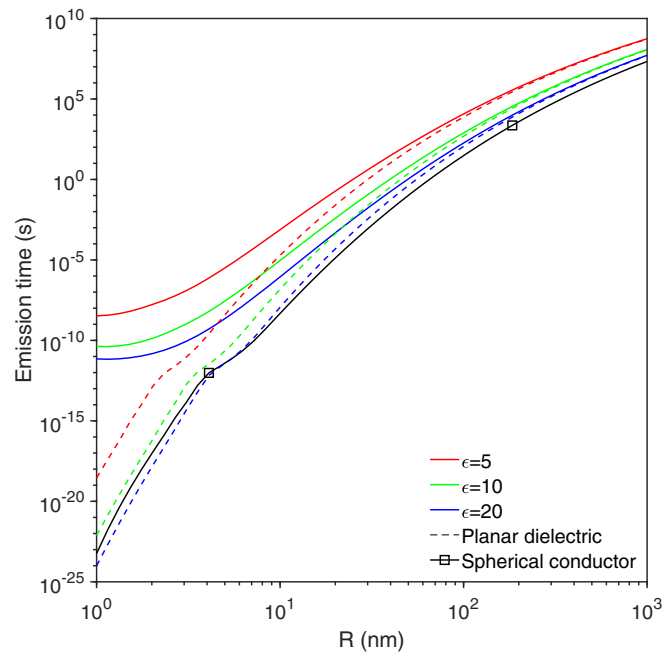

FIG. 5. Time required to evaporate 10% of the charge of a droplet that initially is at the Rayleigh limit. We consider our spherical dielectric model and the previous planar dielectric and spherical conductor models. The liquid temperature is 25 °C, the surface tension is 0.05 J/m^2, and ΔG_0^S is 1.7 eV.

shows that the planar dielectric and spherical conductor models predict substantial energy barrier reductions at zero radius of curvature, and this, coupled with the singular electric field, leads to infinite current densities as well as an infinite total current. In addition to this calculation for the ideal conical geometry, we note that the tips of physical ion-emitting Taylor cones are not infinitely sharp, but instead should end in a spherical cusp with a small but finite radius of a few nanometers. Therefore, the effects of the curvature and the dielectric constant on the reduction of the energy barrier will also be significant in actual Taylor cones, and our model will provide a better estimate of ion emission than the previous planar and spherical conductor models.

A droplet charged above its Rayleigh limit [26],

$$Q_{\mathrm{Ray}} = 8\pi\sqrt{\varepsilon_0 \gamma R^3}, \tag{20}$$

is unstable and will undergo a Coulomb explosion to give rise to smaller, stable droplets [27]. An electrosprayed droplet can reach the Rayleigh limit as its liquid phase evaporates while retaining its net charge, or as a section of the cylindrical jet evolves into the droplet during the jet breakup [21]. If a droplet that is at the Rayleigh limit is small enough, ion evaporation may reduce its charge before it becomes unstable, preventing the Coulomb explosion. We next evaluate the characteristic emission time of a droplet charged at the Rayleigh limit as a function of its radius, using our and previous models for the reduction of the energy barrier. We consider a spherical droplet with its net charge Q distributed on its surface. Conservation of charge, the electric field at the surface, and the ion emission equation

$$\frac{dQ}{dt} = -4\pi R^2 J, \tag{21}$$

$$E_s = \frac{Q}{4\pi\varepsilon_0 R^2}, \tag{22}$$

$$J = \frac{k_B T}{4\pi h}\frac{Q}{R^2}\exp\left(\frac{G(E) - \Delta G_0^S}{k_B T}\right), \tag{23}$$

together with (20) as an initial condition, yield $Q(t)$ as ions are field-emitted. Figure 5 shows the time needed to evaporate 10% of the charge when considering our model and previous models for the reduction of the energy barrier. As expected, the emission time computed with our model (8) converges to the planar model as $R \to \infty$. However, for these large droplets, the field-emitted current is so small and the emission time so large that ion emission is irrelevant. On the other hand, when the droplets are small enough so that ion emission becomes a factor [21], the effect of the radius of curvature is significant. Figure 5 shows that in this case, the use of either the planar dielectric model or the spherical conductor model greatly overestimates the intensity of ion field emission, leading to emission times 2–10 orders of magnitude smaller than those computed with the more physical model that includes the radius of curvature and the dielectric constant

TABLE I. Total current emitted from an ideal Taylor cone for different ion emission models and values of the dielectric constant.

ε	Spherical dielectric	Planar dielectric	Spherical conductor
5	0.014 nA	∞	
10	1.966 nA	∞	∞
20	28.10 nA	∞	

of the droplet. This difference will have a significant impact on the prediction of the distributions of droplets and ions in these complex beams [21].

V. CONCLUSION

The radius of curvature and the dielectric constant of a liquid medium play a significant role in the intensity of ion field emission. We have developed a model that accounts for both factors, and provides an analytical solution for the reduction $G(E)$ of the energy barrier impeding ion emission. Since ion emission is an exponential function of $G(E)$ and typical ion emitting surfaces are characterized by both small radii of curvature and their dielectric nature, the model derived in this article is important for obtaining physical results in actual problems. $G(E)$ is lowered, and therefore ion emission diminished, at decreasing dielectric constant and decreasing radius of curvature. Ion emission from typical systems differs substantially when calculated with either our model or with existing simpler models (which assume an infinite radius of curvature or emission from a perfect conductor). In the case of an ideal Taylor cone, our model yields a finite value for the ion current despite the singular behavior of the electric field at the vertex; conversely, planar or perfect conductor models yield an unphysically infinite ion current. In the case of ion emission from a nanodroplet charged at the Rayleigh limit, the simpler models predict characteristic emission times 2–10 orders of magnitude smaller than the times obtained with our model. It is also worth noting that obtaining the free enthalpy of solution of an ion is a problem of considerable interest [28]. Although ΔG_0^S can be estimated with the continuum Born model [29] and with molecular-dynamics calculations [30,31], a more direct and accurate method involves the use of a well-defined geometry from which the intensity of ion-field emission is measured [11]. The model developed in this article will be important for this direct, experimental measurement of ΔG_0^S, because an error in the calculation of $G(E)$ yields the same error in the determination of ΔG_0^S.

ACKNOWLEDGMENTS

This work was funded by the Air Force Office of Scientific Research, Award No. FA9550-21-1-0200, and an Air Force Research Laboratory grant, Award No. F1SRQ21019M001. We thank the monitors of the programs, Mitat Birkan and Daniel Eckhardt, for their support.

[1] E. W. Müller, Abreißen adsorbierter ionen durch hohe elektrische feldstärken, Naturwissenschaften **29**, 533 (1941).
[2] E. W. Müller, Field desorption, Phys. Rev. **102**, 618 (1956).
[3] R. Gomer, Field emission and field ionization in condensed phases, Acc. Chem. Res. **5**, 41 (1972).
[4] J. B. Fenn, M. Mann, C. K. Meng, S. F. Wong, and C. M. Whitehouse, Electrospray ionization for mass spectrometry of large biomolecules, Science **246**, 64 (1989).
[5] M. Gamero-Castaño and J. de la Mora, Mechanisms of electrospray ionization of singly and multiply charged salt clusters, Anal. Chim. Acta **406**, 67 (2000).
[6] I. Loscertales and J. Fernández De La Mora, Experiments on the kinetics of field evaporation of small ions from droplets, J. Chem. Phys. **103**, 5041 (1995).
[7] X. Gallud and P. C. Lozano, The emission properties, structure and stability of ionic liquid menisci undergoing electrically assisted ion evaporation, J. Fluid Mech. **933**, A43 (2022).
[8] M. Gamero-Castaño, Electric-Field-Induced Ion Evaporation from Dielectric Liquid, Phys. Rev. Lett. **89**, 147602 (2002).
[9] I. Romero-Sanz, R. Bocanegra, J. Fernandez De La Mora, and M. Gamero-Castaño, Source of heavy molecular ions based on taylor cones of ionic liquids operating in the pure ion evaporation regime, J. Appl. Phys. **94**, 3599 (2003).
[10] P. Lozano and M. Martínez-Sánchez, Ionic liquid ion sources: characterization of externally wetted emitters, J. Colloid Interf. Sci. **282**, 415 (2005).
[11] M. Gamero-Castaño and J. Fernandez De La Mora, Direct measurement of ion evaporation kinetics from electrified liquid surfaces, J. Chem. Phys. **113**, 815 (2000).
[12] I. Guerrero, R. Bocanegra, F. J. Higuera, and J. F. De la Mora, Ion evaporation from taylor cones of propylene carbonate mixed with ionic liquids, J. Fluid Mech. **591**, 437 (2007).
[13] C. O'Quinn and K. Jones, Increased access to space with modularity and interface standards, in *AIAA SCITECH 2022 Forum, San Diego* (2022), p. 0647.
[14] J. R. Kopacz, R. Herschitz, and J. Roney, Small satellites an overview and assessment, Acta Astronaut. **170**, 93 (2020).
[15] K. Lemmer, Propulsion for cubesats, Acta Astronaut. **134**, 231 (2017).
[16] I. Levchenko, K. Bazaka, Y. Ding, Y. Raitses, S. Mazouffre, T. Henning, P. J. Klar, S. Shinohara, J. Schein, L. Garrigues *et al.*, Space micropropulsion systems for cubesats and small satellites: From proximate targets to furthermost frontiers, Appl. Phys. Rev. **5**, 011104 (2018).
[17] D. Krejci, F. Mier-Hicks, R. Thomas, T. Haag, and P. Lozano, Emission characteristics of passively fed electrospray microthrusters with propellant reservoirs, J. Spacecr. Rockets **54**, 447 (2017).
[18] D. Krejci, F. Mier-Hicks, C. Fucetola, P. Lozano, A. H. Schouten, and F. Martel, Design and characterization of a scalable ion electrospray propulsion system, in *Proceedings of the IEPC, Kobe, Japan* (2015).
[19] D. Krejci and P. Lozano, Space propulsion technology for small spacecraft, Proc. IEEE **106**, 362 (2018).
[20] J. Iribarne and B. Thomson, On the evaporation of small ions from charged droplets, J. Chem. Phys. **64**, 2287 (1976).
[21] M. Gamero-Castaño and A. Cisquella-Serra, Electrosprays of highly conducting liquids: A study of droplet and ion emission based on retarding potential and time-of-flight spectrometry, Phys. Rev. Fluids **6**, 013701(2021).
[22] J. A. Stratton, *Electromagnetic Theory* (John Wiley & Sons, Hoboken, New Jersey, 2007), Vol. 33.

[23] M.-G. Li, L. Chen, Y.-X. Zhong, Z.-B. Chen, J.-W. Yan, and B.-W. Mao, The electrochemical interface of ag (111) in 1-ethyl-3-methylimidazolium bis (trifluoromethylsulfonyl) imide ionic liquida combined in-situ scanning probe microscopy and impedance study, Electrochim. Acta **197**, 282 (2016).

[24] A. Meyer, The size of molecules, Chem. Soc. Rev. **15**, 449 (1986).

[25] G. Taylor, Disintegration of water drops in an electric field, Proc. R. Soc. London A **280**, 383 (1964).

[26] L. Rayleigh, Xx. On the equilibrium of liquid conducting masses charged with electricity, London, Edinburgh, Dublin Philos. Mag. J. Sci. **14**, 184 (1882).

[27] J. F. De La Mora, On the outcome of the coulombic fission of a charged isolated drop, J. Colloid Interf. Sci. **178**, 209 (1996).

[28] R. Dogonadze, E. Kalman, A. Kornyshev, and J. Ulstrup, *The Chemical Physics of Solvation*, Studies in physical and theoretical chemistry (Elsevier, Amsterdam, 1985).

[29] W. C. Still, A. Tempczyk, R. C. Hawley, and T. Hendrickson, Semianalytical treatment of solvation for molecular mechanics and dynamics, J. Am. Chem. Soc. **112**, 6127 (1990).

[30] A. Nicholls, D. L. Mobley, J. P. Guthrie, J. D. Chodera, C. I. Bayly, M. D. Cooper, and V. S. Pande, Predicting small-molecule solvation free energies: an informal blind test for computational chemistry, J. Med. Chem. **51**, 769 (2008).

[31] D. Shivakumar, Y. Deng, and B. Roux, Computations of absolute solvation free energies of small molecules using explicit and implicit solvent model, J. Chem. Theory Comput. **5**, 919 (2009).